Current Biology
Report

Somatosensory Neurons Enter a State of Altered Excitability during Hibernation

Lydia J. Hoffstaetter,[1,2,3,7] Marco Mastrotto,[1,2,3,7] Dana K. Merriman,[4] Sulayman D. Dib-Hajj,[5,6] Stephen G. Waxman,[5,6] Sviatoslav N. Bagriantsev,[1,*] and Elena O. Gracheva[1,2,3,8,*]
[1]Department of Cellular and Molecular Physiology, Yale University School of Medicine, 333 Cedar St, New Haven, CT 06510, USA
[2]Department of Neuroscience, Yale University School of Medicine, 333 Cedar St, New Haven, CT 06510, USA
[3]Program in Cellular Neuroscience, Neurodegeneration and Repair, Yale University School of Medicine, 333 Cedar St, New Haven, CT 06510, USA
[4]Department of Biology, University of Wisconsin-Oshkosh, 800 Algoma Boulevard, Oshkosh, WI 54901, USA
[5]The Center for Neuroscience and Regeneration Research and Department of Neurology, Yale University School of Medicine, 333 Cedar Street, New Haven, CT 06510, USA
[6]Center for Restoration of Nervous System Function, Veterans Affairs Connecticut Healthcare System, West Haven, CT 06516, USA
[7]These authors contributed equally
[8]Lead Contact
*Correspondence: slav.bagriantsev@yale.edu (S.N.B.), elena.gracheva@yale.edu (E.O.G.)
https://doi.org/10.1016/j.cub.2018.07.020

SUMMARY

Hibernation in mammals involves prolonged periods of inactivity, hypothermia, hypometabolism, and decreased somatosensation. Peripheral somatosensory neurons play an essential role in the detection and transmission of sensory information to CNS and in the generation of adaptive responses. During hibernation, when body temperature drops to as low as 2°C, animals dramatically reduce their sensitivity to physical cues [1, 2]. It is well established that, in non-hibernators, cold exposure suppresses energy production, leading to dissipation of the ionic and electrical gradients across the plasma membrane and, in the case of neurons, inhibiting the generation of action potentials [3]. Conceivably, such cold-induced elimination of electrogenesis could be part of a general mechanism that inhibits sensory abilities in hibernators. However, when hibernators become active, the bodily functions—including the ability to sense environmental cues—return to normal within hours, suggesting the existence of mechanisms supporting basal functionality of cells during torpor and rapid restoration of activity upon arousal. We tested this by comparing properties of somatosensory neurons from active and torpid thirteen-lined ground squirrels (*Ictidomys tridecemlineatus*). We found that torpid neurons can compensate for cold-induced functional deficits, resulting in unaltered resting potential, input resistance, and rheobase. Torpid neurons can generate action potentials but manifest markedly altered firing patterns, partially due to decreased activity of voltage-gated sodium channels. Our results provide insights into the mechanism that preserves somatosensory neurons in a semi-active state, enabling fast restoration of sensory function upon arousal. These findings contribute to the development of strategies enabling therapeutic hypothermia and hypometabolism.

RESULTS AND DISCUSSION

Somatosensory Neurons Retain Action Potential Electrogenesis during Hibernation

We analyzed the electrical properties of dorsal root ganglion (DRG) neurons isolated from active and torpid squirrels (Figure 1A). We focused on thermoreceptors and nociceptors, which in squirrels and other rodents have a soma diameter of less than 30 μm (Figure 1B) [4–6]. To preserve state-specific properties, neurons were incubated at their respective physiological temperatures (37°C for active and 10°C for torpid neurons) prior to patch-clamp recordings at 20°C, the most commonly used temperature for electrophysiological recordings from DRG. Strikingly, we found that, even though squirrels spent 1 or 2 weeks in torpor with body temperature below 10°C, the resting membrane potential (RMP) and input resistance of torpid neurons remained unchanged compared to active neurons (RMP, mean ± SEM: −56.95 ± 1.06 mV and −59.46 ± 1.24 mV for active and torpid neurons, respectively, $p = 0.1302$; input resistance: 883.8 ± 112.9 MΩ and 743.1 ± 101.2 MΩ for active and torpid neurons, respectively, $p = 0.3399$; $n \geq 30$ cells; Figures 1C and 1D). This suggests that the machinery that maintains the ionic gradient remained functional throughout the period of prolonged hypothermia. Direct *in vivo* measurements are needed to confirm this observation in live animals. In contrast, when active squirrel neurons were incubated at 10°C prior to recordings at 20°C, we detected a hyperpolarization of the RMP (mean ± SEM: −56.95 ± 1.06 mV and −61.59 ± 1.15 mV for active and cold-incubated active neurons, respectively; $p = 0.006$; $n \geq 19$ cells) and a two-fold decrease in input resistance (mean ± SEM: 883.8 ± 112.9 MΩ and 398.6 ± 50.7 MΩ for active and cold-incubated active neurons, $p = 0.0038$, respectively;

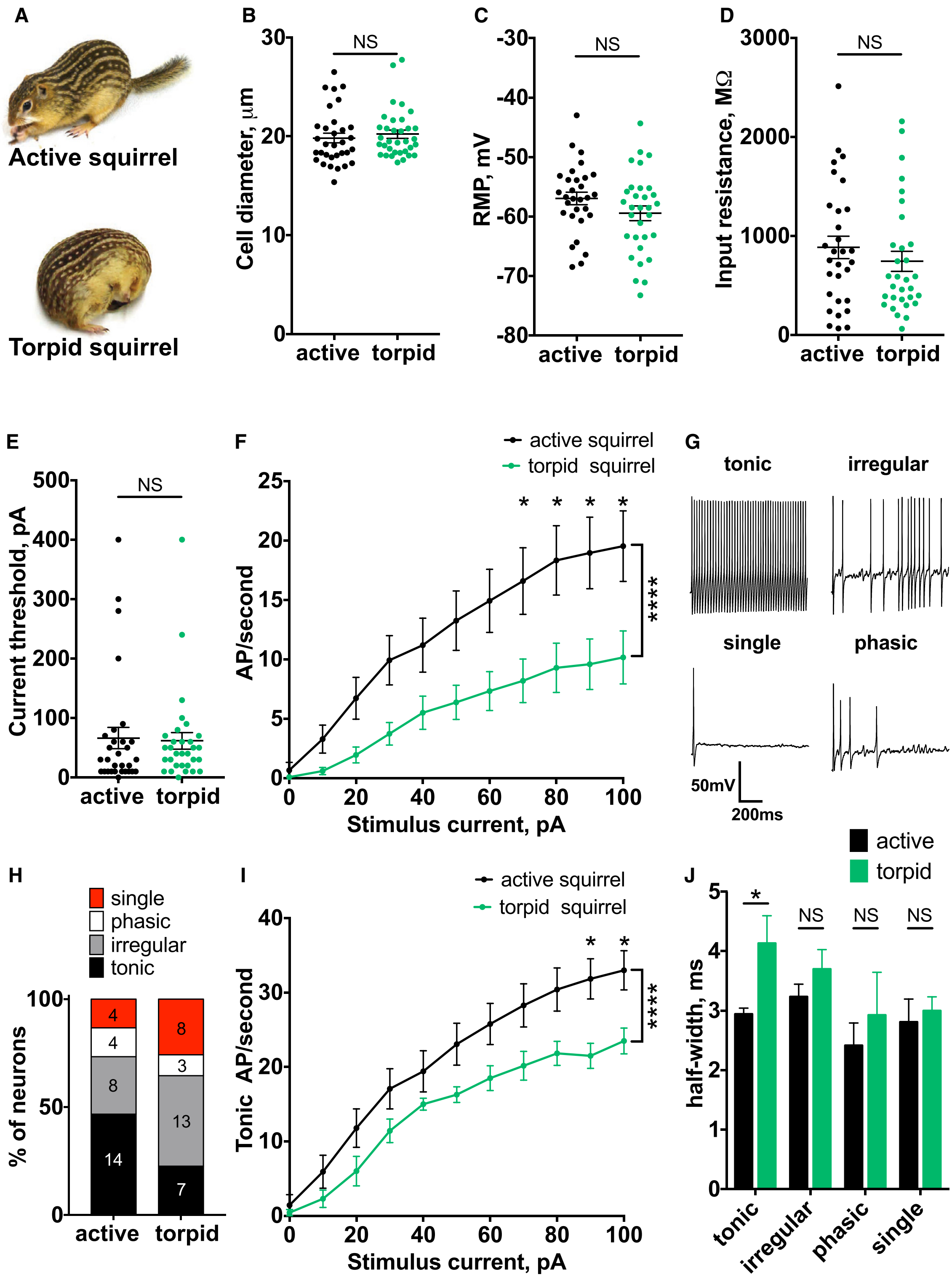

Figure 1. Somatosensory Neurons Retain Action Potential Electrogenesis during Hibernation

(A) Thirteen-lined ground squirrel in the active and torpid state (courtesy of the Gracheva lab).

(B) Diameter of DRG neurons from active and torpid squirrels. NS, not significant; $p > 0.05$; Mann-Whitney U test. Data are shown as mean ± SEM; $n \geq 32$ cells.

(C–E) RMP (C), input resistance (D), and current threshold (E). NS, not significant; $p > 0.05$; unpaired t test (C) and Mann-Whitney U test (D and E). Data are shown as mean ± SEM; $n \geq 30$ cells.

(legend continued on next page)

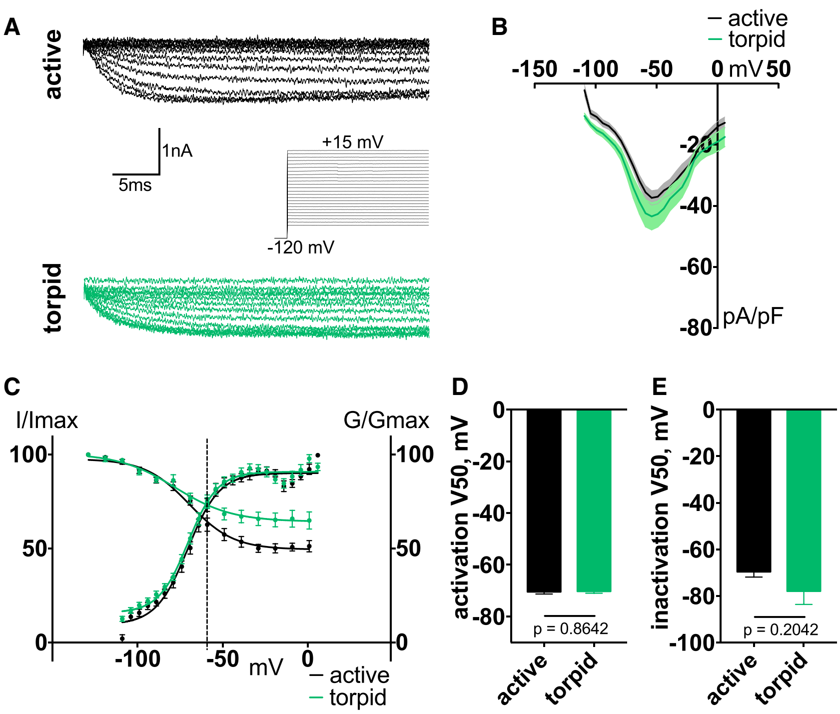

Figure 2. Na_v1.9 Properties Do Not Change during Torpor

(A) Exemplar traces of Na_v1.9-mediated currents with representation of activation protocol in DRG neurons.

(B) Current-voltage relationship of Na_v1.9 from squirrel DRG. Ordinary two-way ANOVA with Bonferroni correction is shown; $p < 0.0001$ main effect between species. Data are shown as mean ± SEM; $n \geq 15$ neurons.

(C) Activation conductance and steady-state inactivation curves of Na_v1.9. Data are shown as mean ± SEM fit with the Boltzmann function. Dashed line indicates average RMP.

(D and E) V_{50} of activation (D) and steady-state inactivation (E), calculated from Boltzmann fit; unpaired t test. Data are shown as mean ± SEM; activation: $n \geq 10$ neurons; inactivation: $n \geq 8$ neurons.

$n \geq 19$ cells; Figures S1A and S1B). Thus, the phenotype observed in torpid neurons does not result from cold exposure alone but rather reflects changes in cellular properties associated with hibernation.

We next examined action potential generation in torpid neurons in response to current injection. Similar to active state, most torpid neurons generated action potentials (30 out of 32 active neurons and 31 out of 34 torpid neurons). Consistent with unchanged RMP and input resistance, both groups required the same amount of current to generate action potentials (mean ± SEM: 66.33 ± 17.88 pA and 61.61 ± 13.99 pA for active and torpid neurons, respectively; $p = 0.3593$; $n \geq 30$ cells; Figure 1E). In contrast, the current threshold was significantly increased in cold-incubated active neurons (mean ± SEM: 88.42 ± 20.75 pA; $p = 0.0345$; $n = 19$ cells; Figure S1C). Increasing current injection elevated the firing frequency in both groups, but torpid neurons had a two- to three-fold lower firing rate (Figure 1F). Thus, although torpid neurons fire at a reduced frequency relative to active neurons, the machinery that generates action potentials remains intact. Overall, our results show that the functionality of somatosensory neurons is suppressed, but not eliminated, during hibernation.

Efficient transmission of sensory information from the periphery to the CNS is encoded in the temporal pattern of somatosensory neuronal firing. The decrease in the overall firing frequency of torpid neurons suggests that, even though action potentials can be generated, the cell-autonomous firing pattern is altered. Consistent with previous studies in rodents [7, 8], we distinguished four groups of cells: with tonic; irregular; phasic; or single firing pattern (Figure 1G). Compared to neurons from active squirrels, torpid neurons showed a two-fold decrease in the proportion of tonically firing cells and a concomitant increase in the fraction of neurons with irregular and single firing (Figure 1H). Tonically firing neurons are the principal transducers of noxious stimuli, including cold [8, 9]. We found that only this group of torpid neurons had reduced firing frequency compared to active cells (Figure 1I), whereas the other groups were not affected (Figure S2). This reduction is likely due to widening of the action potentials, which we detected exclusively in the tonically firing group (half-width, mean ± SEM: 2.94 ± 0.099 ms and 4.13 ± 0.46 ms for active and torpid neurons, respectively; $p = 0.0181$; $n \geq 7$ cells; Figure 1J). Other parameters, including action potential amplitude, afterhyperpolarization, and rise time, remained unchanged in all groups (Figure S3). Consistent with our previous observations, the phenotype observed in torpid neurons did not result from cold exposure alone, because 10°C incubation of active neurons significantly affected all measured action potential parameters (Figure S1D).

A decrease in firing rate in small-diameter nociceptors during hibernation suggests an impairment of the action potential

(F) Action potential (AP) firing rate at increasing current injections from 0 to 100 pA. Ordinary two-way ANOVA with Bonferroni correction is shown; ****$p < 0.0001$ main effect between species; *$p < 0.05$. Data are shown as mean ± SEM; $n \geq 30$ cells.

(G) Exemplar traces of tonic, irregular, single, and phasic firing patterns.

(H) Distribution of firing patterns in active and torpid DRG neurons. Number of cells in each group is indicated.

(I) Firing rate of tonically firing cells at increasing current injections from 0 to 100 pA. Ordinary two-way ANOVA with Bonferroni correction is shown; ****$p < 0.0001$ main effect between species; *$p < 0.05$. Data are shown as mean ± SEM; $n \geq 7$ neurons.

(J) Half-width of action potentials grouped by firing pattern. NS, not significant; $p > 0.05$; *$p < 0.05$, regular two-way ANOVA with Bonferroni correction. Data are shown as mean ± SEM; $n \geq 7$ tonic, $n \geq 8$ irregular, $n \geq 3$ phasic, and $n \geq 4$ single.

See also Figures S1–S3.

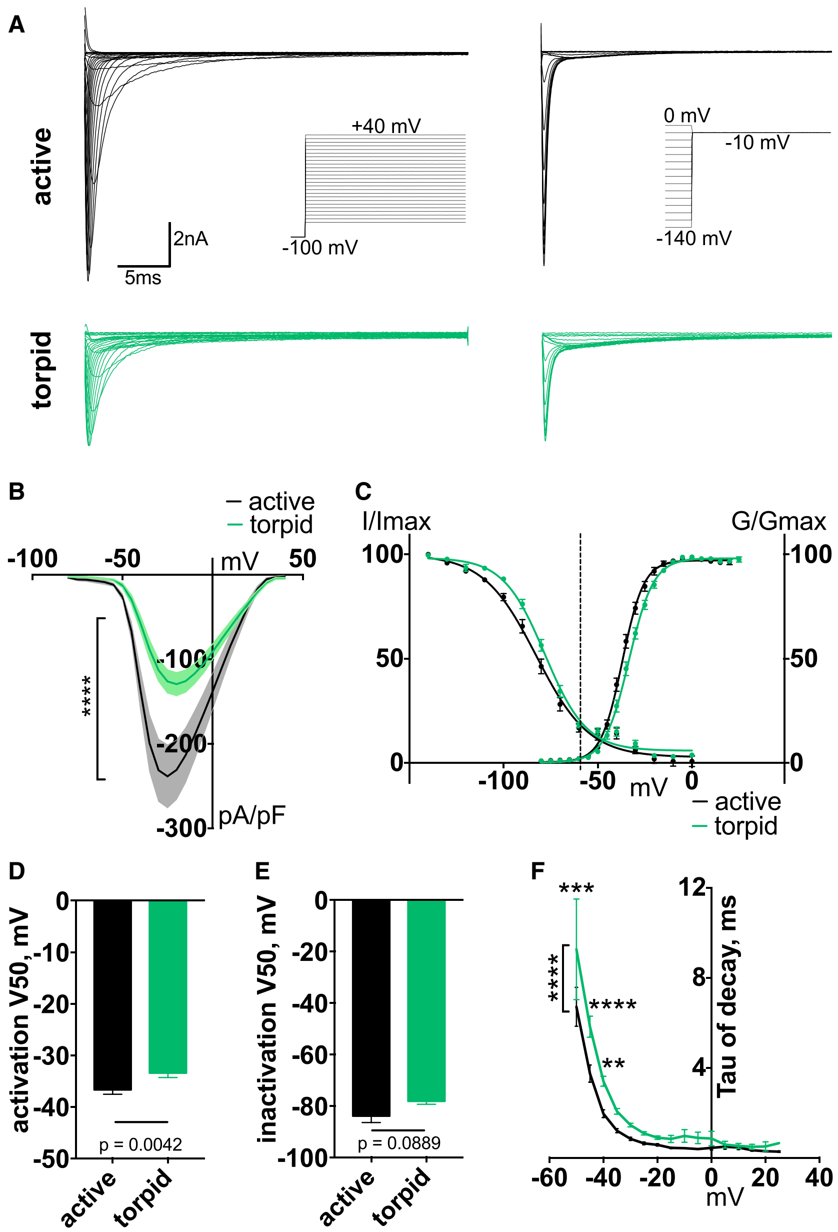

Figure 3. TTX-S Current Density Is Reduced during Torpor

(A) Exemplar current traces and voltage protocols for activation (left) and steady-state inactivation (right) of TTX-S currents in DRG neurons.

(B) Voltage dependence of TTX-S current. Ordinary two-way ANOVA with Bonferroni correction is shown; ****$p < 0.0001$ main effect between species. Data are shown as mean ± SEM; $n \geq 17$ neurons.

(C) Activation conductance and steady-state inactivation of TTX-S current. Data are shown as mean ± SEM fit with Boltzmann functions. Dashed line indicates average RMP.

(D and E) V_{50} of activation (D) and steady-state inactivation (E), averaged from individual Boltzmann fits; Mann-Whitney U test. Data are shown as mean ± SEM; $n \geq 16$ neurons.

(F) Inactivation rate (tau of decay), calculated from a single-exponential curve fit to the decay of the current at each voltage. Only curves fit with an $R^2 > 0.95$ were included. Ordinary two-way ANOVA with Bonferroni correction is shown; $p < 0.0001$ main effect between species. **$p < 0.01$; ***$p < 0.001$; ****$p < 0.0001$. Data are shown as mean ± SEM; n = 5–18 active; n = 2–17 torpid neurons.

See also Figure S4.

generation machinery. A similar reduction in firing rate was observed in tonically firing mouse DRG neurons as a result of knockout of $Na_v1.8$, a major voltage-gated sodium channel in C-type nociceptors [7]. Therefore, to understand the molecular basis of the impaired action potential electrogenesis during torpor, we sought to investigate the activity of voltage-gated sodium channels in DRG neurons.

Somatosensory Neurons from Hibernating Squirrels Have Decreased Na_v Activity

In the majority of thermoreceptors and nociceptors, action potentials are mainly (though not exclusively) generated and propagated by a triad of voltage-gated sodium channels: $Na_v1.9$; $Na_v1.7$; and $Na_v1.8$ [10–19]. $Na_v1.9$ is activated at the most hyperpolarized potentials and generates persistent non-inactivating currents, contributing to setting the RMP and the threshold for action potentials [20–23]. $Na_v1.7$ is responsible for the initial phase of action potential, leading to the rapid depolarizing upstroke produced by $Na_v1.8$ [7, 24–26]. We hypothesized, based on our observation of reduced firing rate and redistribution of firing patterns, that torpid neurons have altered Na_v channel function.

Using a protocol developed for recording tetrodotoxin-resistant (TTX-R) $Na_v1.9$ current in rodent DRG [27], we recorded a sodium current with similar characteristics in squirrel DRG neurons, suggesting it is mediated by the squirrel ortholog of $Na_v1.9$. We found no differences in $Na_v1.9$ current density, voltage dependence of activation, and steady-state inactivation between active and torpid neurons (V_{50} of activation, mean ± SEM: −70.46 ± 0.83 mV and −70.27 ± 0.73 mV for active and torpid neurons, respectively, p = 0.8642, $n \geq 15$ cells; V_{50} of inactivation: −69.55 ± 2.31 mV and −77.89 ± 5.71 mV for active and torpid neurons, respectively, p = 0.2042, $n \geq 9$ cells; Figure 2). Of note, compared to $Na_v1.9$ orthologs from other mammals, $Na_v1.9$ from active and torpid neurons showed little inactivation, even at positive potentials. Overall, these data are consistent with unchanged RMP and current threshold (Figures 1C and 1E).

$Na_v1.7$ is a tetrodotoxin-sensitive (TTX-S) channel that contributes to ~70% of the total TTX-S current in mouse DRG [28–30]. The voltage-dependence and kinetics of $Na_v1.7$ enable the channel to amplify subthreshold depolarization and set the

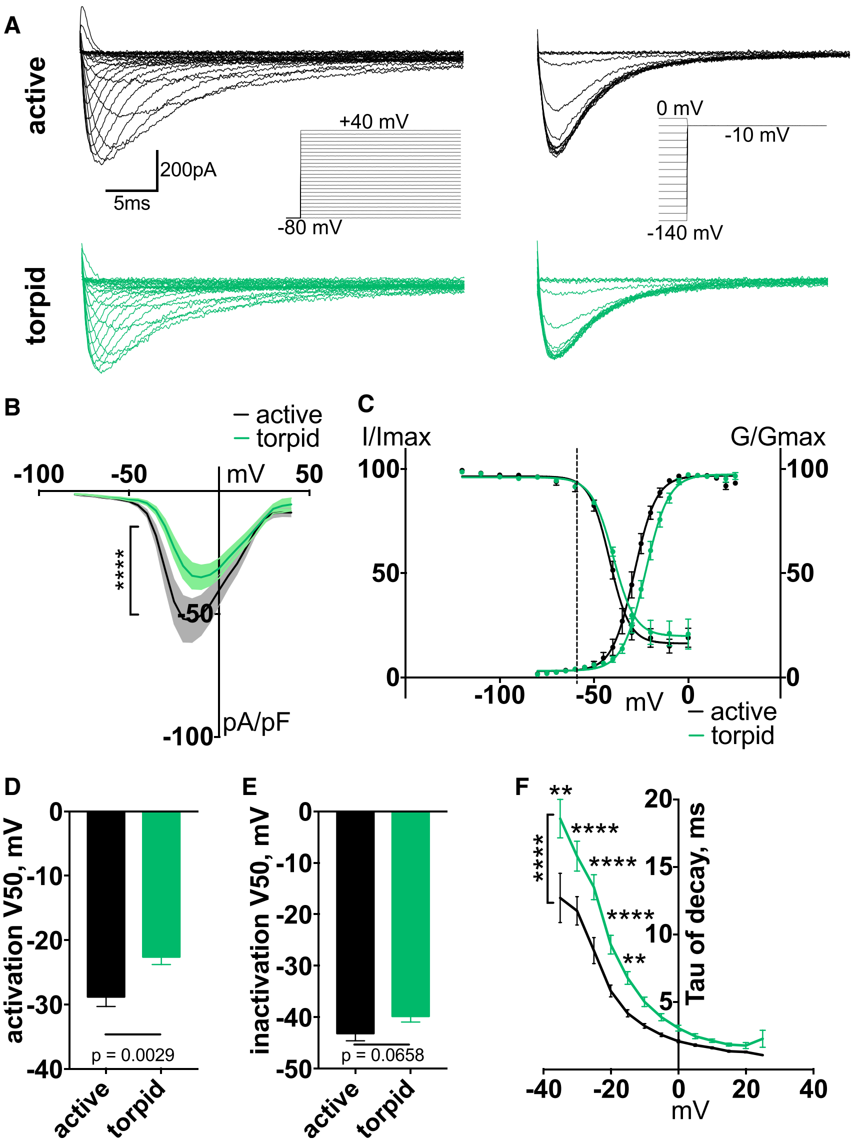

Figure 4. $Na_v1.8$ Current Activation Is Depolarized during Torpor

(A) Exemplar current traces and voltage protocols for activation (left) and steady-state inactivation (right) of $Na_v1.8$ currents in DRG neurons.

(B) Current-voltage relationship of $Na_v1.8$. Ordinary two-way ANOVA with Bonferroni correction is shown; ****$p < 0.0001$ main effect between species. Data are shown as mean ± SEM; $n \geq 14$ cells.

(C) Activation conductance and steady-state inactivation of $Na_v1.8$. Data are shown as mean ± SEM fit with Boltzmann functions. Dashed line indicates average RMP.

(D and E) V_{50} of activation (D) and steady-state inactivation (E), averaged from individual Boltzmann fits; unpaired t test (D) and Mann-Whitney U test (E). Data are shown as mean ± SEM; $n \geq 12$ neurons.

(F) Inactivation rate (tau of decay), calculated from a single-exponential curve fit to the decay of the current at each voltage. Only curves fit with an $R^2 > 0.95$ were included. Ordinary two-way ANOVA with Bonferroni correction is shown; $p < 0.0001$ main effect between species. **$p < 0.01$; ****$p < 0.0001$. Data are shown as mean ± SEM; n = 4–13 active; n = 2–15 torpid neurons.

See also Figure S4.

gain on the sensitivity of somatosensory neurons [31]. We found a ~50% decrease of TTX-S current density in torpid neurons compared to active (Figures 3A and 3B). We also detected a small depolarizing shift in the voltage dependence of activation but no change in steady-state fast inactivation (V_{50} of activation, mean ± SEM: −36.68 ± 0.87 mV and −33.43 ± 0.87 mV for active and torpid neurons, respectively, p = 0.0042, $n \geq 17$ cells; V_{50} of inactivation: −83.95 ± 2.55 mV and −78.18 ± 1.21 mV for active and torpid neurons, respectively, p = 0.0889, $n \geq 16$ cells; Figures 3C–3E). As a result of the change in V_{50} of activation, torpid neurons exhibited a significant prolongation of TTX-S current decay (Figures 3F and S4A). The substantially decreased density of the TTX-S current from torpid neurons is expected to prolong the initial phase of the action potential, leading to a decreased firing rate [32].

We next measured $Na_v1.8$-mediated TTX-R current in DRG neurons. Similar to $Na_v1.7$, torpid neurons exhibited a significant reduction in $Na_v1.8$ current density (Figures 4A and 4B) and a profound 6-mV depolarizing shift in the voltage dependence of activation (V_{50} of activation, mean ± SEM: −28.81 ± 1.49 mV and −22.61 ± 1.19 mV for active and torpid neurons, respectively; p = 0.0029; $n \geq 14$ cells; Figures 4C and 4D). The voltage dependence of steady-state inactivation remained unchanged (V_{50} of inactivation, mean ± SEM: −43.13 ± 1.45 mV and −39.8 ± 1.13 mV for active and torpid neurons, respectively; p = 0.0658; $n \geq 12$ cells; Figures 4C and 4E). Consistent with a shift in V_{50} of activation, we also detected a significant prolongation of the rate of $Na_v1.8$ current decay (Figures 4F and S4B). The depolarizing shift in activation of $Na_v1.8$ is expected to suppress the probability of firing in torpid neurons, and slower inactivation might contribute to increased action potential width.

Cumulatively, 95% of active and torpid DRG neurons contained both TTX-S and TTX-R currents, demonstrating that $Na_v1.7$ and $Na_v1.8$ are present in the majority of neurons from both groups (Figure S4C). The decrease in the amplitude of the two currents in torpid neurons could be due to diminished gene expression. However, we found only a small (~20%) reduction in $Na_v1.7$ message in torpid neurons and no change in $Na_v1.8$ message (Figures S4D and S4E), suggesting other regulatory mechanisms, which remain to be determined.

Conclusions

Our study revealed several unexpected findings: (1) during torpor, somatosensory neurons preserve general electrical properties—RMP, input resistance, and rheobase—indistinguishable from the active state; (2) electrical properties of torpid neurons reflect complex changes associated with hibernation and cannot be recapitulated by merely exposing active neurons to cold; (3) torpid neurons retain the action-potential-generating machinery; and (4) firing of torpid neurons shifts from tonic to irregular and single, suggesting suppressed action potential generation, likely due to the observed changes in functional properties of the Na_vs, which could arise from alternative splicing, posttranslational modifications, interaction with auxiliary proteins, and/or changes in the plasma membrane. We do not rule out potential contribution from voltage-gated potassium channels, which remains to be determined.

Our results show that the somatosensory system does not undergo complete shutdown during hibernation. Instead, somatosensory neurons employ cold-resistant machineries to maintain ionic gradients and electrical potentials similar to the active state. These processes are energetically expensive, underscoring the notion that torpor is an active physiological process that requires molecular fine-tuning. Indeed, recent studies in hibernating rodents revealed profound genomically encoded changes in temperature sensors, mitochondrial function, protein control machineries, and cytoskeletal integrity [5, 6, 33]. We suggest the existence of other such modifications in various groups of enzymes, ion channels, and transporters implicated in energy homeostasis and ionic balance regulation.

The preservation of action-potential-generating machinery in the somatosensory system during torpor may be beneficial for the animal as it emerges from hibernation and re-establishes the essential means of communication with its environment. The quick restoration of sensory abilities requires such machinery to be in a functional or semi-functional state rather than *de novo* synthesis and assembly. It appears possible that similar principles could be at work in other systems and organs of mammalian hibernators.

STAR★METHODS

Detailed methods are provided in the online version of this paper and include the following:

- KEY RESOURCES TABLE
- CONTACT FOR REAGENT AND RESOURCE SHARING
- EXPERIMENTAL MODEL AND SUBJECT DETAILS
  - Animals
  - Primary neuron dissociation
  - Patch-clamp electrophysiology
  - qPCR
- QUANTIFICATION AND STATISTICAL ANALYSIS

SUPPLEMENTAL INFORMATION

Supplemental Information includes four figures and can be found with this article online at https://doi.org/10.1016/j.cub.2018.07.020.

ACKNOWLEDGMENTS

We thank Karen Tonsfeldt for performing preliminary experiments and members of the Gracheva and Bagriantsev laboratories for their contributions throughout the project. This study was partly funded by the Beckman Foundation, Rita Allen Foundation, and NIH grant 1R01NS091300-01A1 to E.O.G.; National Science Foundation (NSF) CAREER grant 1453167 and NIH grant 1R01NS097547-01A1 to S.N.B.; and by the Axle Tech International Endowed Professorship to D.K.M.

AUTHOR CONTRIBUTIONS

L.J.H., M.M., E.O.G., and S.N.B. designed and performed experiments and collected and analyzed data. D.K.M. supplied squirrels and provided advice on animal husbandry. S.D.D.-H. and S.G.W. provided guidance for data analysis. L.J.H., S.N.B., and E.O.G. wrote the manuscript with contributions from all authors. E.O.G. and S.N.B. conceived the study and provided guidance and supervision throughout the project.

DECLARATION OF INTERESTS

The authors declare no competing interests.

Received: June 3, 2018
Revised: June 28, 2018
Accepted: July 6, 2018
Published: August 30, 2018

REFERENCES

1. Carey, H.V., Andrews, M.T., and Martin, S.L. (2003). Mammalian hibernation: cellular and molecular responses to depressed metabolism and low temperature. Physiol. Rev. *83*, 1153–1181.
2. Geiser, F. (2013). Hibernation. Curr. Biol. *23*, R188–R193.
3. Boutilier, R.G. (2001). Mechanisms of cell survival in hypoxia and hypothermia. J. Exp. Biol. *204*, 3171–3181.
4. Harper, A.A., and Lawson, S.N. (1985). Conduction velocity is related to morphological cell type in rat dorsal root ganglion neurones. J. Physiol. *359*, 31–46.
5. Laursen, W.J., Schneider, E.R., Merriman, D.K., Bagriantsev, S.N., and Gracheva, E.O. (2016). Low-cost functional plasticity of TRPV1 supports heat tolerance in squirrels and camels. Proc. Natl. Acad. Sci. USA *113*, 11342–11347.
6. Matos-Cruz, V., Schneider, E.R., Mastrotto, M., Merriman, D.K., Bagriantsev, S.N., and Gracheva, E.O. (2017). Molecular prerequisites for diminished cold sensitivity in ground squirrels and hamsters. Cell Rep. *21*, 3329–3337.
7. Renganathan, M., Cummins, T.R., and Waxman, S.G. (2001). Contribution of Na(v)1.8 sodium channels to action potential electrogenesis in DRG neurons. J. Neurophysiol. *86*, 629–640.
8. Yu, Y.Q., Chen, X.F., Yang, Y., Yang, F., and Chen, J. (2014). Electrophysiological identification of tonic and phasic neurons in sensory dorsal root ganglion and their distinct implications in inflammatory pain. Physiol. Res. *63*, 793–799.
9. Zimmermann, K., Leffler, A., Babes, A., Cendan, C.M., Carr, R.W., Kobayashi, J., Nau, C., Wood, J.N., and Reeh, P.W. (2007). Sensory neuron sodium channel Nav1.8 is essential for pain at low temperatures. Nature *447*, 855–858.
10. Akopian, A.N., Sivilotti, L., and Wood, J.N. (1996). A tetrodotoxin-resistant voltage-gated sodium channel expressed by sensory neurons. Nature *379*, 257–262.
11. Akopian, A.N., Souslova, V., England, S., Okuse, K., Ogata, N., Ure, J., Smith, A., Kerr, B.J., McMahon, S.B., Boyce, S., et al. (1999). The tetrodotoxin-resistant sodium channel SNS has a specialized function in pain pathways. Nat. Neurosci. *2*, 541–548.
12. Amaya, F., Decosterd, I., Samad, T.A., Plumpton, C., Tate, S., Mannion, R.J., Costigan, M., and Woolf, C.J. (2000). Diversity of expression of the sensory neuron-specific TTX-resistant voltage-gated sodium ion channels SNS and SNS2. Mol. Cell. Neurosci. *15*, 331–342.

13. Catterall, W.A., Goldin, A.L., and Waxman, S.G. (2005). International Union of Pharmacology. XLVII. Nomenclature and structure-function relationships of voltage-gated sodium channels. Pharmacol. Rev. *57*, 397–409.

14. Dib-Hajj, S., Black, J.A., Cummins, T.R., and Waxman, S.G. (2002). NaN/Nav1.9: a sodium channel with unique properties. Trends Neurosci. *25*, 253–259.

15. Toledo-Aral, J.J., Moss, B.L., He, Z.J., Koszowski, A.G., Whisenand, T., Levinson, S.R., Wolf, J.J., Silos-Santiago, I., Halegoua, S., and Mandel, G. (1997). Identification of PN1, a predominant voltage-dependent sodium channel expressed principally in peripheral neurons. Proc. Natl. Acad. Sci. USA *94*, 1527–1532.

16. Sangameswaran, L., Fish, L.M., Koch, B.D., Rabert, D.K., Delgado, S.G., Ilnicka, M., Jakeman, L.B., Novakovic, S., Wong, K., Sze, P., et al. (1997). A novel tetrodotoxin-sensitive, voltage-gated sodium channel expressed in rat and human dorsal root ganglia. J. Biol. Chem. *272*, 14805–14809.

17. Djouhri, L., Newton, R., Levinson, S.R., Berry, C.M., Carruthers, B., and Lawson, S.N. (2003). Sensory and electrophysiological properties of guinea-pig sensory neurones expressing Nav 1.7 (PN1) Na+ channel alpha subunit protein. J. Physiol. *546*, 565–576.

18. Dib-Hajj, S.D., Tyrrell, L., Black, J.A., and Waxman, S.G. (1998). NaN, a novel voltage-gated Na channel, is expressed preferentially in peripheral sensory neurons and down-regulated after axotomy. Proc. Natl. Acad. Sci. USA *95*, 8963–8968.

19. Hoffstaetter, L.J., Bagriantsev, S.N., and Gracheva, E.O. (2018). TRPs et al.: a molecular toolkit for thermosensory adaptations. Pflugers Arch. *470*, 745–759.

20. Herzog, R.I., Cummins, T.R., and Waxman, S.G. (2001). Persistent TTX-resistant Na+ current affects resting potential and response to depolarization in simulated spinal sensory neurons. J. Neurophysiol. *86*, 1351–1364.

21. Priest, B.T., Murphy, B.A., Lindia, J.A., Diaz, C., Abbadie, C., Ritter, A.M., Liberator, P., Iyer, L.M., Kash, S.F., Kohler, M.G., et al. (2005). Contribution of the tetrodotoxin-resistant voltage-gated sodium channel NaV1.9 to sensory transmission and nociceptive behavior. Proc. Natl. Acad. Sci. USA *102*, 9382–9387.

22. Lolignier, S., Bonnet, C., Gaudioso, C., Noël, J., Ruel, J., Amsalem, M., Ferrier, J., Rodat-Despoix, L., Bouvier, V., Aissouni, Y., et al. (2015). The Nav1.9 channel is a key determinant of cold pain sensation and cold allodynia. Cell Rep. *11*, 1067–1078.

23. Cummins, T.R., Dib-Hajj, S.D., Black, J.A., Akopian, A.N., Wood, J.N., and Waxman, S.G. (1999). A novel persistent tetrodotoxin-resistant sodium current in SNS-null and wild-type small primary sensory neurons. J. Neurosci. *19*, RC43.

24. Choi, J.S., and Waxman, S.G. (2011). Physiological interactions between Na(v)1.7 and Na(v)1.8 sodium channels: a computer simulation study. J. Neurophysiol. *106*, 3173–3184.

25. Rush, A.M., Cummins, T.R., and Waxman, S.G. (2007). Multiple sodium channels and their roles in electrogenesis within dorsal root ganglion neurons. J. Physiol. *579*, 1–14.

26. Matsutomi, T., Nakamoto, C., Zheng, T., Kakimura, J., and Ogata, N. (2006). Multiple types of Na(+) currents mediate action potential electrogenesis in small neurons of mouse dorsal root ganglia. Pflugers Arch. *453*, 83–96.

27. Cummins, T.R., Rush, A.M., Estacion, M., Dib-Hajj, S.D., and Waxman, S.G. (2009). Voltage-clamp and current-clamp recordings from mammalian DRG neurons. Nat. Protoc. *4*, 1103–1112.

28. Ho, C., and O'Leary, M.E. (2011). Single-cell analysis of sodium channel expression in dorsal root ganglion neurons. Mol. Cell. Neurosci. *46*, 159–166.

29. Gingras, J., Smith, S., Matson, D.J., Johnson, D., Nye, K., Couture, L., Feric, E., Yin, R., Moyer, B.D., Peterson, M.L., et al. (2014). Global Nav1.7 knockout mice recapitulate the phenotype of human congenital indifference to pain. PLoS ONE *9*, e105895.

30. Vasylyev, D.V., Han, C., Zhao, P., Dib-Hajj, S., and Waxman, S.G. (2014). Dynamic-clamp analysis of wild-type human Nav1.7 and erythromelalgia mutant channel L858H. J. Neurophysiol. *111*, 1429–1443.

31. Dib-Hajj, S.D., Yang, Y., Black, J.A., and Waxman, S.G. (2013). The Na(V) 1.7 sodium channel: from molecule to man. Nat. Rev. Neurosci. *14*, 49–62.

32. Alexandrou, A.J., Brown, A.R., Chapman, M.L., Estacion, M., Turner, J., Mis, M.A., Wilbrey, A., Payne, E.C., Gutteridge, A., Cox, P.J., et al. (2016). Subtype-selective small molecule inhibitors reveal a fundamental role for Nav1.7 in nociceptor electrogenesis, axonal conduction and presynaptic release. PLoS ONE *11*, e0152405.

33. Ou, J., Ball, J.M., Luan, Y., Zhao, T., Miyagishima, K.J., Xu, Y., Zhou, H., Chen, J., Merriman, D.K., Xie, Z., et al. (2018). iPSCs from a hibernator provide a platform for studying cold adaptation and its potential medical applications. Cell *173*, 851–863.e16.

34. Laursen, W.J., Mastrotto, M., Pesta, D., Funk, O.H., Goodman, J.B., Merriman, D.K., Ingolia, N., Shulman, G.I., Bagriantsev, S.N., and Gracheva, E.O. (2015). Neuronal UCP1 expression suggests a mechanism for local thermogenesis during hibernation. Proc. Natl. Acad. Sci. USA *112*, 1607–1612.

STAR★METHODS

KEY RESOURCES TABLE

REAGENT OR RESOURCE	SOURCE	IDENTIFIER
Experimental Models: Organisms/Strains		
Thirteen-lined ground squirrel: *Ictidomys tridecemlineatus*	University of Wisconsin Oshkosh	N/A
Oligonucleotides		
sqScn9a Fwd ATCCCAGCCTCACAGTGACAG	This paper	N/A
sqScn9a Rev CACTCAGAGGAACTCAATCGGC	This paper	N/A
sqScn10a Fwd CTGCAGCAAGTCGGGAGGTA	This paper	N/A
sqScn10a Rev TGCAGGAACCTGAGGAGCAG	This paper	N/A
HPRT1 Fwd TGATAGATCCATTCTATGACTGTAGA	This paper	N/A
HPRT1 Rev CAACAATCAAGACATTCTTTCCA	This paper	N/A
Software and Algorithms		
Prism 7	GraphPad	https://www.graphpad.com/how-to-buy/
ImageJ	NIH	https://imagej.nih.gov/ij/download.html
Pclamp	Molecular Devices	http://mdc.custhelp.com/app/answers/detail/a_id/20260/~/axon%E2%84%A2-pclamp%E2%84%A2-11-electrophysiology-data-acquisition-%26-analysis-software
MATLAB	MathWorks	https://www.mathworks.com/downloads/

CONTACT FOR REAGENT AND RESOURCE SHARING

Further information and requests for resources and reagents should be directed to Elena O. Gracheva (elena.gracheva@yale.edu).

EXPERIMENTAL MODEL AND SUBJECT DETAILS

Animals

Animals were housed in a pathogen-free facility at Yale University. All animal procedures were performed in compliance with the Office of Animal Research Support of Yale University (protocol 2018-11497). Thirteen-lined ground squirrels were maintained on a diet of dog food (Iams) supplemented with sunflower seeds, superworms, and fresh vegetables. During the summer active period, squirrels were individually housed on a 12-h light/dark cycle with *ad libitum* access to food and water. During the winter torpid period, squirrels were individually housed in a specialized facility at 4°C ambient temperature and constant dark.

Primary neuron dissociation

Primary neurons were dissected from dorsal root ganglia of active and torpid squirrels (~1 year old). Active animals were euthanized via CO_2 inhalation followed by decapitation. Dorsal root ganglia were dissected into ice-cold HBSS. Tissue was then briefly treated with collagenase P (1mg/mL in HBSS, 15 min, 37°C) followed by 0.25% trypsin (10 min, 37°C). Finally, tissue was suspended in Hibernate-A media (with custom osmolarity at 280 mOsm) supplemented with B-27 supplement and glutaMAX (GIBCO) according to the manufacturer's recommendation (adjusted to pH 8.0 with NaOH). Hibernate-A media is designed to have a stable pH at ambient levels of CO_2. Tissue was mechanically dissociated using a plastic tipped pipette before being plated on poly-D-lysine coated coverslips (Corning) at room temperature for 30 s and immediately placed at 37°C in 0.3% CO_2, or at 10°C in 0.3% CO_2 for cold incubation. Torpid animals were euthanized by decapitation. Torpid dorsal root ganglia were dissociated identically to active tissues, but were subsequently incubated at 10°C in 0.3% CO_2. Small diameter neurons (< 30 μm) were selected for recording after becoming adherent (~2hrs), for up to 36 hr after plating.

Patch-clamp electrophysiology

Solutions and protocols were based on methods previously described [27]. Data were acquired on a Zeiss Axio-Examiner with an Orca flash 4.0 camera (Hamamatsu) and an Axopatch 200-B amplifier/Digidata 1440 digitizer (Molecular Devices). Recordings were acquired using pCLAMP software (Molecular Devices) sampled at 20-50 kHz and low-pass filtered at 2–10 kHz. Experiments were carried out at a room temperature of 22–25°C. Coverslips that were incubated at 37°C were placed into the recording chamber with bath solutions at room temperature, and several neurons were patched on the same coverslip for up to 1 hr. In order to minimize effects of acute warming of cold-incubated cells, coverslips that were incubated at 10°C were placed into the recording chamber with bath solutions cooled to 10°C. Only after a suitable neuron was identified was the bath solution warmed to room temperature, the cell was patched within 5 min of warming and was kept only for the duration of the recording protocol, in some cases up to 30 min.

Current-clamp experiments were performed with DRG neurons collected from summer active squirrels between end of May to beginning of August (n = 8), or from winter torpid squirrels between October and March (n = 5). The internal pipette solution consisted of (in mM): 140 KCl, 0.5 EGTA, 5 HEPES, and 3 Mg-ATP (adjusted to pH 7.3 with KOH, osmolarity adjusted to 300 mOsm with dextrose). External solution contained (in mM): 140 NaCl, 3 KCl, 2 $MgCl_2$, and 10 HEPES (adjusted to pH 7.3 with NaOH, osmolarity adjusted to 315 mOsm with dextrose). Patch pipettes of borosilicate glass with an o.d. of 1.5 mm (Warner Instruments no. G150F-3) were pulled and polished to a tip resistance of 1.3–3 MΩ using a P-1000 puller (Sutter Instruments) and CPM-2 (ALA Scientific Instruments) microforge. Liquid junction potentials (5 mV) were corrected offline. Immediately after whole-cell recording was established, resting membrane potential was measured in I = 0 mode. Cells with a resting potential of lower than −40 mV were not included in the dataset. Input resistance was calculated by recording voltage changes by injection of 5 pA depolarizing currents. Action potential firing was elicited through sequential 1 s steps of depolarizing currents from 0-200 pA in 10 pA increments. If a cell did not fire in this range, current steps were gradually increased to up to 80 pA increments for up to 20 steps. Characteristics of the action potential waveform were determined using custom scripts in MATLAB (MathWorks Inc). Action potential amplitude was measured from peak maximum to after-hyperpolarization minimum. Action potential half-width was measured from the rising phase to the falling phase at 1/2 the amplitude. Rise time was measured from 20%–80% of the peak maximum. An image of each neuron was recorded, and neuron diameter was measured in ImageJ (NIH) as the average of the long and short axes.

Voltage-clamp experiments were performed with DRG neurons collected from active squirrels (n = 8) or torpid squirrels (n = 6) as described above. The internal pipette solution consisted of (in mM): 140 CsF, 10 NaCl, 2 $MgCl_2$, 0.1 $CaCl_2$, 1.1 EGTA, 10 HEPES (adjusted to pH 7.2 with CsOH, osmolarity adjusted to 310 mOsm with dextrose). External solution contained (in mM): 140 NaCl, 3 KCl, 1 $MgCl_2$, 1 $CaCl_2$, 10 HEPES, 10 dextrose (adjusted to pH 7.3 with NaOH, osmolarity adjusted to 320 mOsm with dextrose). To isolate sodium currents, 20 mM TEA-Cl (blocks voltage-gated K^+ channels), and 0.1 mM $CdCl_2$ (blocks voltage-gated Ca^{2+} channels) were added to the external solution. Due to very large TTX-S currents produced by squirrel neurons, recordings of TTX-S and Nav1.8 were performed with a low-sodium external solution in which the NaCl concentration was replaced with 35 mM NaCl and 105 mM Choline-Cl. Patch pipettes were pulled and polished to a tip resistance of 1–2 MΩ. Cells with a seal > 1GΩ and a leak current < 200 pA were used for recordings. 85% series resistance compensation was used to minimize voltage errors. Linear leak subtraction was applied to all recordings, using P/6 (Nav1.9 recordings) or P/4 (TTX-S and Nav1.8 recordings) hyperpolarizing control pulses applied after the depolarizing test stimuli.

Nav1.9 currents were isolated by adding 250 nM tetrodotoxin (TTX) to the external solution and holding at hyperpolarized potentials (−120 mV). Only the persistent currents of the resulting recordings were extracted, to avoid the Nav1.8-mediated component. The peak persistent current was measured from a visually determined window where the non-persistent current has decayed while the persistent current remains constant. For activation, 200-ms pulses were used from −100 mV to +15 mV, in 5 mV steps. For steady-state fast inactivation, 200-ms prepulses from – 140 mV to +10 mV, in 10 mV steps were used, followed by a 150-ms test pulse to 0 mV. Measurements of Nav1.9 current were corrected for liquid junction potentials offline (9 mV).

TTX-S currents were isolated by performing sequential recordings in the absence and in the presence of 250 nM TTX. The TTX-R residual current was subtracted from the total sodium current to obtain the TTX-S component. Holding potential was −100 mV. For activation, 100-ms pulses were used from −80 mV to +40 mV, in 5 mV steps. For steady-state fast inactivation 100-ms prepulses from −140 mV to 0 mV, in 10 mV steps were used, followed by a 100-ms test pulse to −10 mV.

Nav1.8 currents were isolated by applying 250 nM TTX and holding at depolarized potentials (−80 mV), at which Nav1.9 in the presence of CsF becomes inactivated. These recordings were performed in sequence with the recording of TTX-S currents, making it possible to evaluate the co-distribution of Nav1.8 and TTX-S. For activation, 100-ms pulses were used from −80 mV to +40 mV, in 5 mV steps. For steady-state fast inactivation, 100-ms prepulses from −140 mV to 0 mV, in 10 mV steps were used, followed by a 100-ms test pulse to −10 mV. Measurements of TTX-S, and Nav1.8 were corrected for liquid junction potentials (8 mV) online.

qPCR

Total RNA was extracted from squirrel DRG using the TRIzol reagent (Invitrogen). One microgram of total RNA was used to synthesize cDNA using the qScript cDNA Supermix (95048; Quanta Biosciences). qPCR calibrations and normalizations were performed using the Illumina Eco System machine in accordance with the manufacturer's instructions. Each reaction was run in triplicate, using the HPRT1 gene as the reference [34]. Amplification primer pairs (5′–3′) were Scn9a: ATCCCAGCCTCACAGTGACAG; CACTCAGAG GAACTCAATCGGC (product size 133 bp); Scn10a: CTGCAGCAAGTCGGGAGGTA; TGCAGGAACCTGAGGAGCAG (product size 109 bp).

QUANTIFICATION AND STATISTICAL ANALYSIS

Data were obtained from at least two independent experiments and analyzed with GraphPad Prism 7.0 (GraphPad Software), and the number of experimental points is indicated in each figure. Activation conductance g_m was calculated from the equation $g_m = I_{Na}/(E_m-E_{rev})$, where I_{Na} is the peak current, E_m is the corresponding voltage, and E_{rev} is the estimated reversal potential.

To calculate the midpoints (V_{50}) of activation and steady-state fast inactivation, activation conductance was normalized and plotted against the corresponding voltage step, and test-pulse-evoked inactivation current was normalized and plotted against the corresponding conditioning pulse. The resulting curves were fit by a Boltzmann function in Prism 7 (GraphPad). The inactivation rate (tau of decay) was calculated by fitting the decaying component of the current at each voltage to a single-exponential equation ($I = \Delta I^{*}\exp^{\wedge}(-t/\tau_{inact})$, where ΔI is the difference between peak sodium current and baseline, t is the time from the peak current, the start of the fit, and τ_{inact} is the decay constant) using MATLAB (MathWorks). Only curves fit with an $R^2 > 0.95$ were included.

Statistical tests were chosen based on the distribution of the data: unpaired Student's t test for normally distributed data (D'Agostino & Pearson normality test), with Welch's correction for data with statistically different variances (F test), Mann-Whitney U test for not normally distributed data. Regular 2-way ANOVAs were corrected for multiple comparisons using Bonferroni correction.

Report

Current Biology

Somatosensory Neurons Enter a State of Altered Excitability during Hibernation

Highlights

- Hibernating DRG neurons have unchanged resting potential, resistance, and rheobase
- Hibernating DRG neurons retain electrogenicity, with decreased firing rate
- Properties of hibernating neurons are innate and not triggered by cold alone
- Properties of hibernating neurons are dictated by altered Na_v channel function

Authors

Lydia J. Hoffstaetter, Marco Mastrotto, Dana K. Merriman, Sulayman D. Dib-Hajj, Stephen G. Waxman, Sviatoslav N. Bagriantsev, Elena O. Gracheva

Correspondence

slav.bagriantsev@yale.edu (S.N.B.), elena.gracheva@yale.edu (E.O.G.)

In Brief

Hoffstaetter et al. show that somatosensory neurons from hibernating squirrels exist in a semi-functional state, with decreased ability to generate action potential, partially due to altered activity of Na_v channels. This state reflects complex changes associated with hibernation and cannot be recapitulated by merely exposing active neurons to cold.

Hoffstaetter et al., 2018, Current Biology *28*, 2998–3004
September 24, 2018
https://doi.org/10.1016/j.cub.2018.07.020

Current Biology, Volume *28*

Supplemental Information

Somatosensory Neurons Enter a State of Altered Excitability during Hibernation

Lydia J. Hoffstaetter, Marco Mastrotto, Dana K. Merriman, Sulayman D. Dib-Hajj, Stephen G. Waxman, Sviatoslav N. Bagriantsev, and Elena O. Gracheva

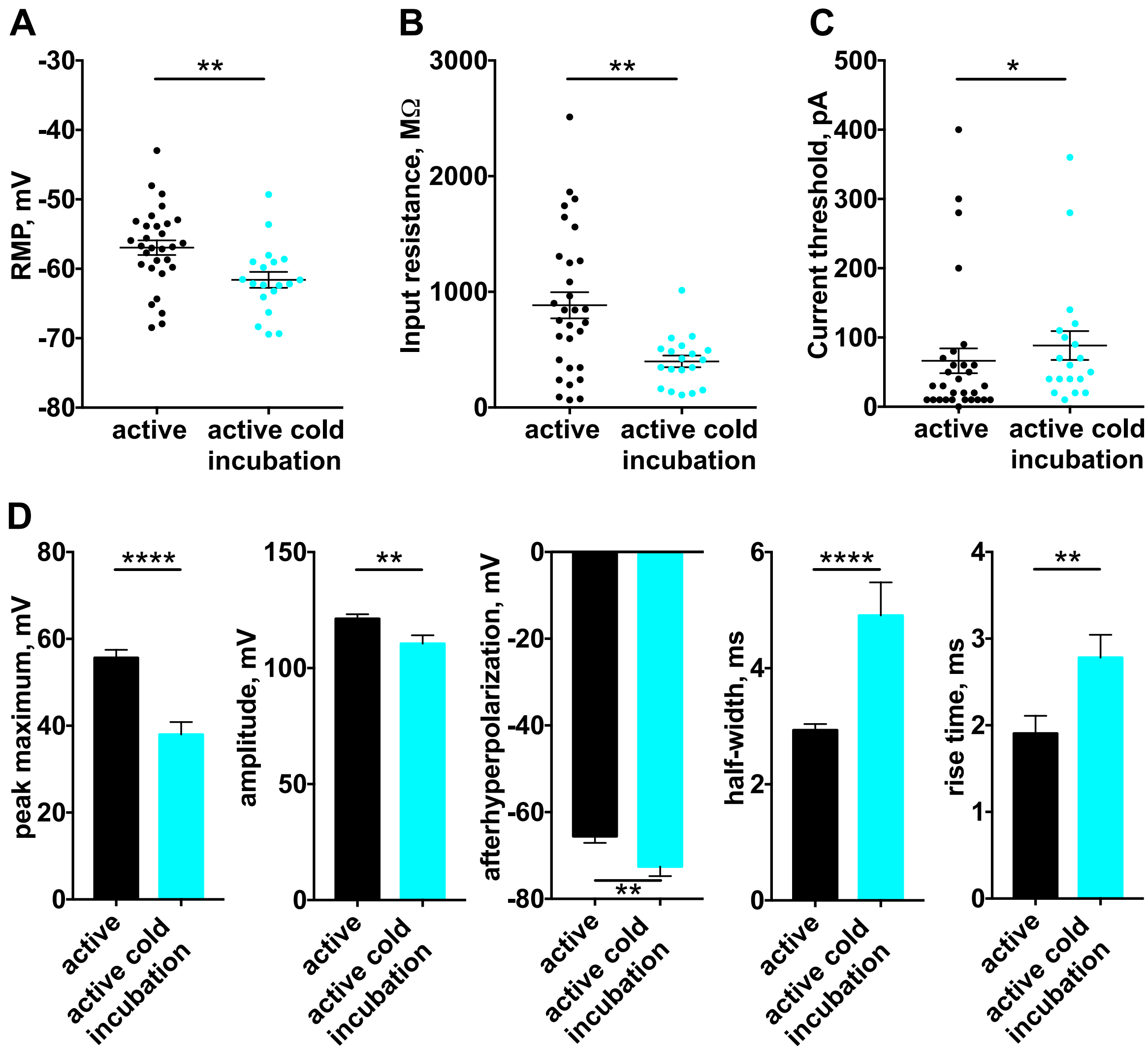

Figure S1. Cold incubation of active neurons changes their electrogenic properties. Related to Figure 1. (A-D) Resting membrane potential (A), input resistance (B), current threshold (C) and action potential parameters (D) obtained from active neurons incubated at 37°C (active) or at 10°C (active cold incubation), *p<0.05, **p<0.01, ****p<0.0001, unpaired t-test (A, D) and Mann-Whitney *U* test (B-D). Data shown as mean ± s.e.m, n≥19 neurons.

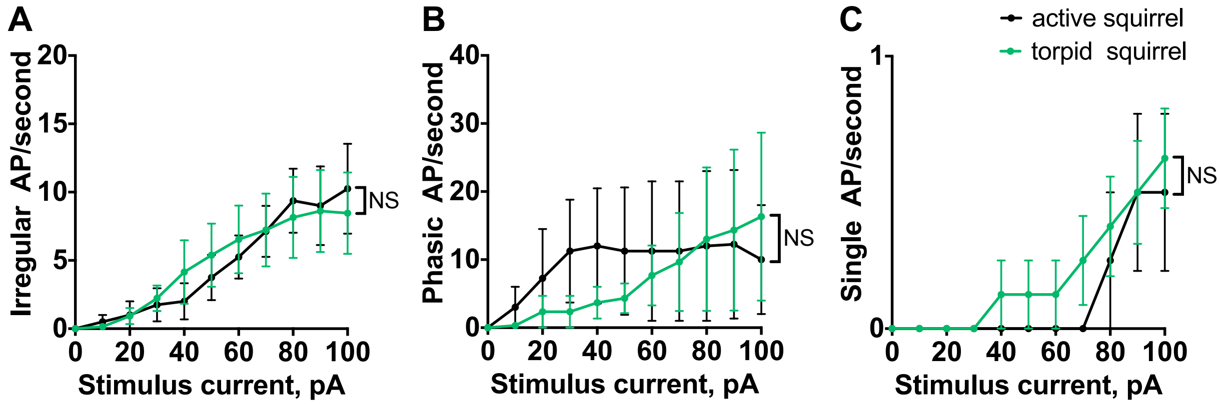

Figure S2. Firing rate of neurons with irregular, phasic, and single firing patterns. Related to Figure 1. Action potential (AP) firing rate at increasing current injections from 0-100 pA. Ordinary two-way ANOVA with Bonferroni correction, NS, not significant; $p>0.05$. Data shown as mean ± s.e.m; n≥8 irregular, n≥3 phasic, n≥4 single.

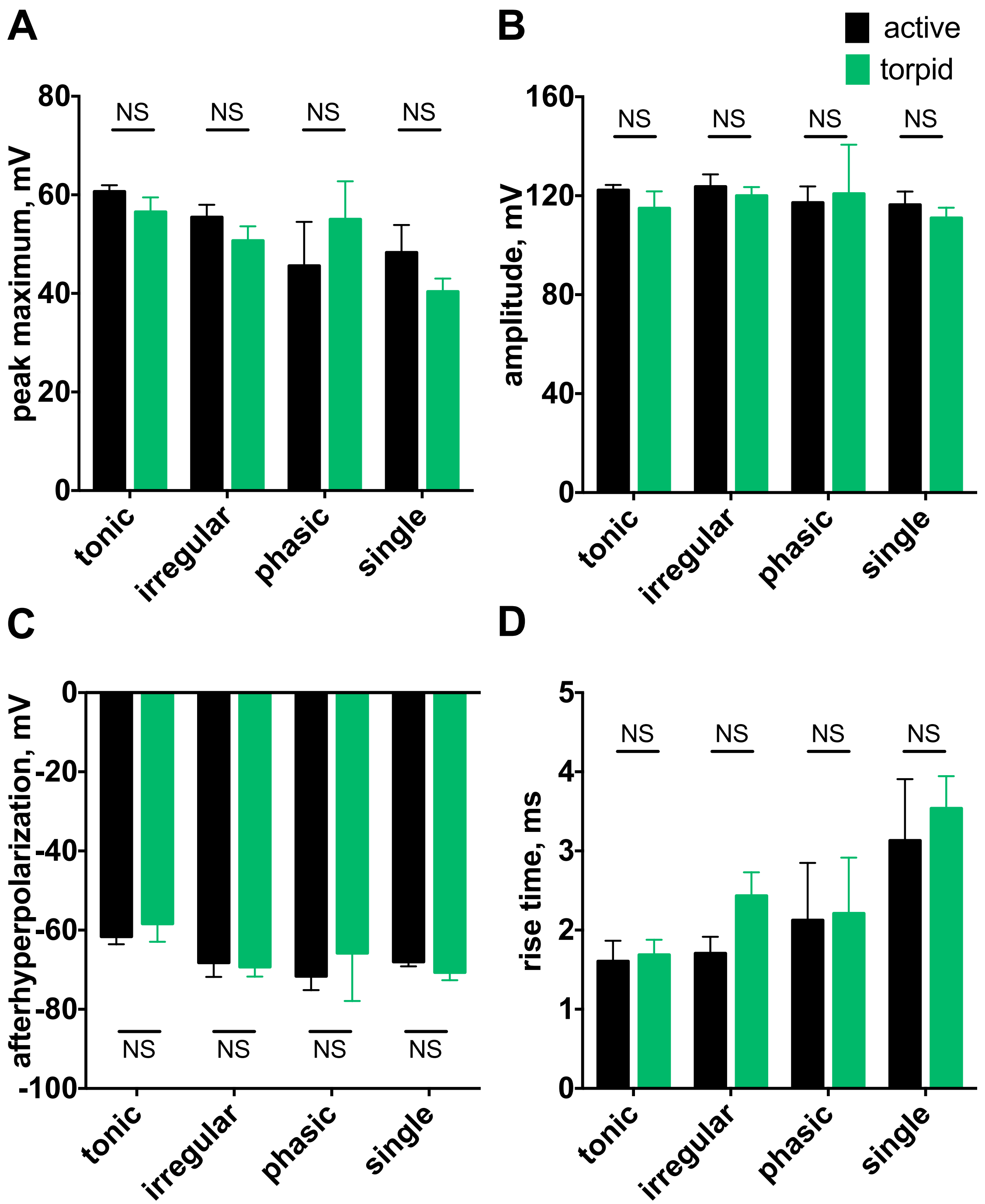

Figure S3. Most action potential properties are unchanged during hibernation. Related to Figure 1. (A-D) Action potential properties grouped by firing pattern: peak maximum (A), amplitude (B), minimum of afterhyperpolarization (C), rise time from 20-80% of peak (D). NS, not significant; $p>0.05$, regular two-way ANOVA with Bonferroni correction. Data shown as mean ± s.e.m; $n \geq 7$ tonic, $n \geq 8$ irregular, $n \geq 3$ phasic, $n \geq 4$ single.

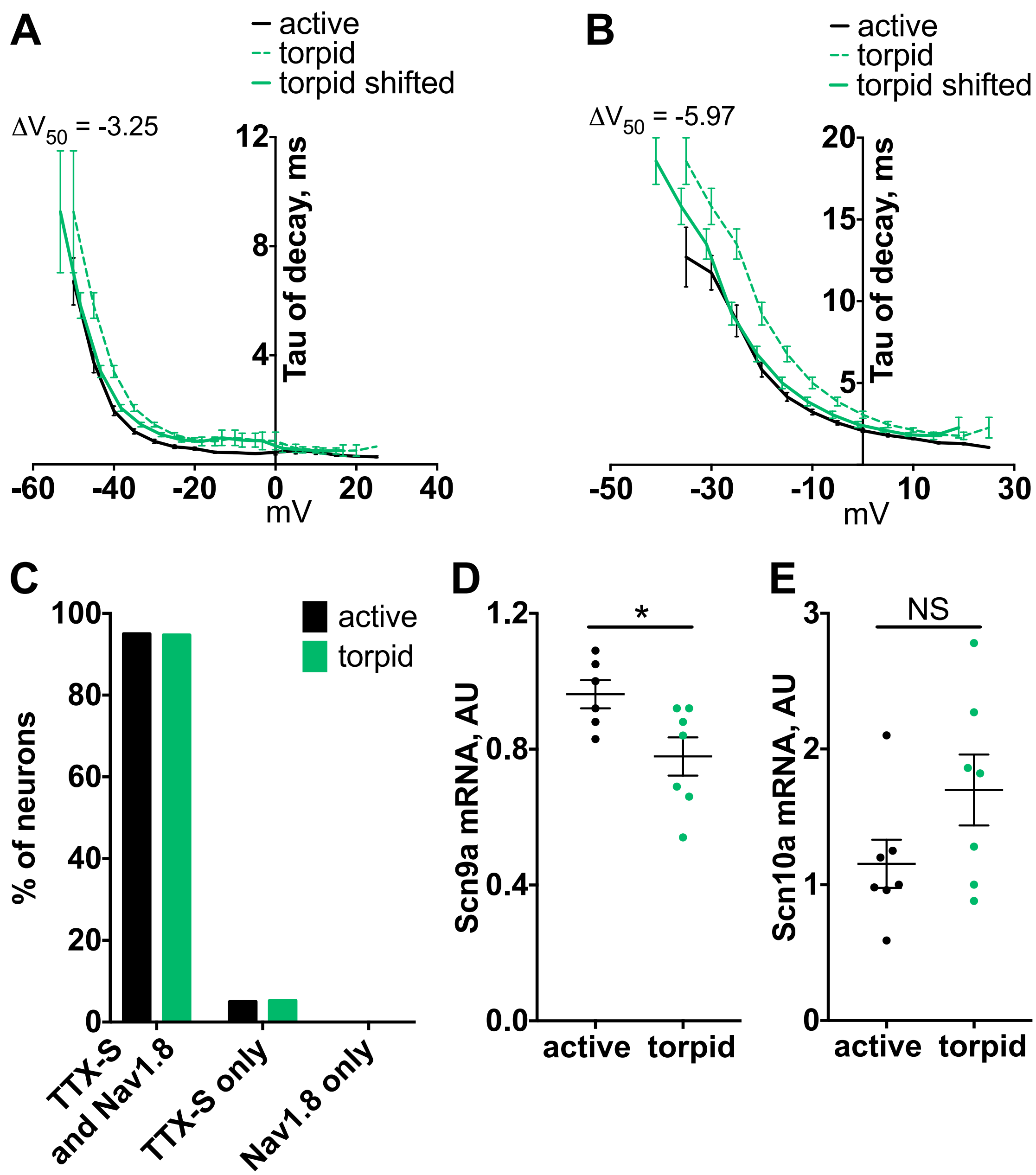

Figure S4. TTX-S and Nav1.8 decay kinetics and expression. Related to Figures 3-4. (A and B) Inactivation rate (tau of decay), calculated from a single-exponential curve fit to the decay of the current at each voltage, and corrected for the indicated difference in V_{50} between conditions. (C) Distribution of Nav1.8 and TTX-S currents in active and torpid DRG neurons. (D, E) Quantitative PCR of *Scn9a* (gene name for Nav1.7) (D) and *Scn10a* (gene name for Nav1.8) transcripts (E) from mRNA isolated from active and torpid squirrel DRG. NS, not significant; $p>0.05$, *$p<0.05$, unpaired t-test. Data shown as mean ± s.e.m, n=6-7 squirrels.